THE JOURNAL OF PHYSICAL CHEMISTRY B

pubs.acs.org/JPCB Article

Solvation in Ionic Liquids with Polymer-Grafted Nanoparticles

Siqi Liu, Mia Walton, Nadezda V. Tarakina, and Pinar Akcora*

Cite This: https://dx.doi.org/10.1021/acs.jpcb.0c02813 Read Online

ACCESS | Metrics & More | Article Recommendations | Supporting Information

ABSTRACT: Polymer-grafted nanoparticles stabilized in ionic liquid (IL)−solvent mixtures are investigated by using transmission electron microscopy, dynamic light scattering, and electrochemical impedance spectroscopy. The ionic conductivity of IL−solvent mixtures with the polymer-grafted nanoparticles is found to be higher than that of nanoparticles in the IL. These particles offer additional interactions between polymer and IL, which can mitigate solvation in ILs with solvents. Motivated by this, we present the conductivity data of 1-hexyl-3-methylimidazolium bis(trifluoromethylsulfonyl)imide (HMIM-TFSI) with poly(methyl methacrylate) (PMMA)-grafted particles in good and bad solvents and further discuss how graft density influences the swelling of PMMA and solvation characteristics of HMIM-TFSI. We found that HMIM-TFSI−acetonitrile containing high grafting density particles has a higher conductivity than that of the HMIM-TFSI−methanol mixture with grafted particles. Thus, solubility of PMMA in acetonitrile and preferential interactions between PMMA−HMIM-TFSI are shown to govern the swelling, solvation, and conductive properties of IL with the polymer-grafted nanoparticles.

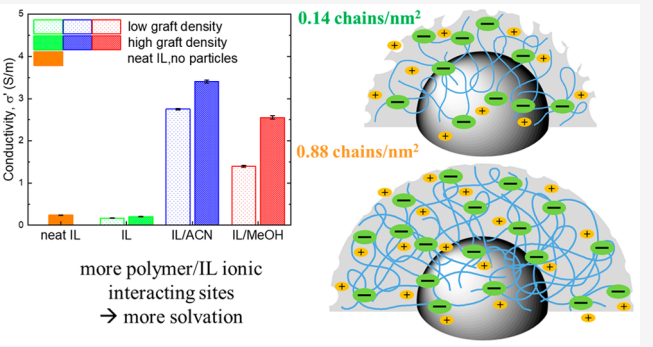

INTRODUCTION

Ionic liquids (ILs) have unique physicochemical properties of negligible vapor pressure, nonflammability, low viscosity, thermal stability, high ionic conductivity, and a wide electrochemical stability window, enabling their uses for sustainable energy, separation, and biomedicine applications.[1−6] ILs are also used in stabilization of nanoparticles through polymer grafting or hydrogen bonding between particles and IL.[7−16] Colloidal gels and glasses of poly(methyl methacrylate) (PMMA)-grafted nanoparticles in IL have been studied for their optical and rheological properties.[17−21] Polymer-grafted nanoparticles in ILs provide solid-like mechanical properties and liquid-like high ionic conductivity to colloidal gels, which are used as solid electrolytes in batteries.[22,23] It was shown that PMMA-grafted silica particles at high concentrations form colloidal crystal structures in IL.[24] In polymer-grafted nanoparticles, the interplay between polymer−solvent and polymer−IL can govern the extent of IL solvation. In this work, the solvation of 1-hexyl-3-methylimidazolium bis(trifluoromethylsulfonyl)imide (HMIM-TFSI) with the addition of solvents of varying polarity with and without PMMA-grafted iron oxide nanoparticles is examined through measuring ionic conductivity in electrochemical impedance spectroscopy. In addition, a series of high-resolution electron microscopy images were analyzed to determine the roughness and thickness of brushes in IL with different graft densities.

Adding imidazolium salts to polymers enhances the thermal stability and decreases the glass transition temperature of a polymer.[25−27] Ion dipole interactions between the $TFSI^-$ anion and PMMA can self-dissociate the EMIM-TFSI, leading to an increase in the number of free cation carriers.[27,28] We hypothesize that this preferential interaction between PMMA and $TFSI^-$ anions can contribute to the solvation of IL with the addition of solvents. The competing interactions between polymer−IL and solvent−IL, thus, determine the ion mobility and diffusion. Mixing ILs with solvents of different polarities alters viscosity and enhances the ion mobility and ionic conductivity in IL-based complex electrolytes as the polar solvent disassociates the ion pairs.[29−33]

In our recent work, we demonstrated that PMMA coupling with HMIM-TFSI enhanced the long-range $HMIM^+$ cation dynamics.[34] Moreover, the long-range cation diffusion was found to be significantly lower in close-packed particles compared to well-dispersed particles, and the confinement of HMIM-TFSI within the aggregated particles dominated the fast process, resulting in the highest constrained diffusion. The cation diffusion mechanism in the grafted particle structures

Received: March 30, 2020
Revised: May 8, 2020
Published: May 18, 2020

substantiated the polymer coupling phenomenon, which improved the ion mobility in polymer grafted-particle based electrolytes. This work is designed to address the role of polymer swelling on solvation of HMIM-TFSI−solvent mixtures to explain the ionic conductivity results. We will use "IL" instead of HMIM-TFSI in the rest of the paper.

METHODS

Sample Preparation. 4-Cyanopentanoic acid dithiobenzoate (CPDB), diethyl ether, oleic acid (90%), and oleylamine (70% technical grade) were purchased from Sigma-Aldrich. Tetrahydrofuran (THF) and cyclohexane (both ACS grades) were purchased from Pharmco-AAPER. 2,2′-Azobis(isobutyronitrile) (AIBN; 98% technical grade) was recrystallized from methanol. HMIM-TFSI was purchased from Iolitec. Inc. All other chemicals were used as received.

Nanoparticle Synthesis. Fe_3O_4 nanoparticles of 22.4 ± 1.4, 28.4 ± 5.1, and 6.5 ± 1.3 nm in diameter were synthesized by the high-temperature thermal decomposition method. The synthetic procedure of larger nanoparticles capped with oleic acid includes two steps:[35] synthesis of iron−oleate complex by ion exchange of iron chloride and sodium oleate salts and thermal decomposition of the iron−oleate precursor. The one-step reaction of 6.5 ± 1.3 nm nanoparticles utilizes iron(III) acetylacetonate, $Fe(acac)_3$, as a precursor and uses both oleic acid and oleylamine as surface ligands[36] which results in nanoparticles at high yields with no byproducts. Particle size and distributions were obtained by analyzing the TEM data in ImageJ through sampling over hundreds of particles.

Preparation of CPDB-Anchored Fe_3O_4 Nanoparticles. CPDB (10 mg/mL in THF) was added dropwise into nanoparticle solution of 20 mg/mL and sonicated in a bath sonicator. The mixture was stirred at room temperature for 24 h. Particles were washed following the previously reported protocol to remove excess CPDB.[37] The mixture was precipitated by adding a large amount of cyclohexane and ethyl ether (4:1 volume ratio), centrifuged at 3000 rpm for 15 min, and redissolved in 25 mL of THF. The washing procedure was repeated three times.

Surface-Initiated Reversible Addition−Fragmentation Chain-Transfer (SI-RAFT) Polymerization of MMA on Fe_3O_4 Nanoparticles. CPDB-anchored Fe_3O_4 particles, MMA, and AIBN in THF solution were degassed in three freeze−pump−thaw cycles. The flask was placed in an oil bath and stirred at 60 °C for 6 h. The flask was immersed in ice water to terminate the polymerization via quenching. To purify the grafted particles, ethanol was added to the solution and centrifuged at 6000 rpm. The washing step was repeated several times until the supernatant solution was clear after addition of ethanol. The supernatant was removed, and particles were redissolved in THF. This procedure was repeated several times to remove the free PMMA chains.

Weight losses of polymer-grafted particles were measured in a thermogravimetric analyzer (Q50 TGA, TA Instruments), and the grafting densities were calculated as reported in the previous work.[38] The weight-averaged molecular weight (M_w) of PMMA grafted on larger particles was determined by using a gel permeation chromatography−light scattering (GPC/LS) device after etching the particles. The GPC/LS system in our laboratory is equipped with a VARIAN PL 5.0 μm Mixed-C gel column (7.5 mm i.d.), a light scattering detector (miniDawn, Wyatt Technology), and a refractive index (RI) detector (Optilab rEX, Wyatt). The weight-averaged molecular weight (M_w) of PMMA grafted on 6.5 nm particles was determined by using an EcoSEC RI-UV GPC with RI detector running at 0.3 mL/min, located at Columbia University. Samples used in this study are listed in Table 1.

Table 1. Characteristics of Grafted PMMA Chains (M_w and $Đ$), Graft Densities, and Particle Core Sizes

grafted chain M_w (kDa)	$Đ$	grafting density, σ (chains/nm^2)	grafting density, σ (chains/nanoparticle)	particle diameter (nm)
42.2	1.15	0.14	19	6.5 ± 1.3
31.2	1.34	0.88	117	6.5 ± 1.3
185.0	1.12	0.05	127	28.4 ± 5.1
159.0	1.17	0.14	355	28.4 ± 5.1
122.7	1.05	0.7	1103	22.4 ± 1.4

Transmission Electron Microscopy (TEM). We collected the TEM data by using two instruments: a FEI TITAN THEMIS 200 TEM located at the CUNY-ASRC Imaging Facility operating at 200 kV and a double Cs corrected JEOL JEM-ARM200F (S)TEM operated at 80 kV and equipped with a cold-field emission gun and a high-angle silicon drift energy dispersive X-ray (EDX) detector (solid angle up to 0.98 steradians with a detection area of 100 mm^2) at the Max Planck Institute of Colloids and Interfaces, Germany. PMMA-grafted particles in HMIM-TFSI−solvent mixtures were drop-cast on lacey carbon grids.

Electrochemical Impedance Spectroscopy (EIS). Bulk ionic conductivity was measured by using EIS from Bio-Logic Science Instruments with model number SP-300. 0.3 mL solutions of HMIM-TFSI and solvent mixtures were placed into a tube with two stainless-steel electrodes. AC impedance measurements were performed at room temperature. An alternating current signal with 10 mV amplitude was applied in the frequency (ω) range of 1 kHz−1 MHz. The real component of the complex conductivity, σ', was calculated via the equation[39] $\sigma'(\omega) = \frac{Z'(\omega)}{k[(Z'(\omega))^2 + (Z''(\omega)^2]}$. The real and imaginary impedance, Z' and Z'', were obtained from the high-frequency plateau, where ionic mobility dominates the impedance spectra.[40] The conductivity cell constant, k, was determined by using 0.01 M KCl standard (Ricca Chemical, 1412 μS/cm at 25 °C).

Dynamic Light Scattering (DLS). The autocorrelation function $g_2(t)$ of scattered intensity measured in DLS was fitted by using the $g_2(t) = A + B\exp(-2\Gamma t)$ equation to obtain the decay constant, $\Gamma = \frac{1}{\tau}$. A is the background designated by the baseline value, B is an instrument factor, t is the time interval, and τ is the relaxation time. Fickian diffusivity is simply obtained from $\Gamma = q^2 D_t$, and the relaxation time (τ) is the inverse of the decay constant. The hydrodynamic radius (r) of grafted particles was calculated by using the Stokes−Einstein equation, $D_t = \frac{k_B T}{6\pi\eta r}$.

A Zetasizer NanoS instrument (Malvern Instruments) was equipped with a He−Ne laser (wavelength λ = 633 nm and a detector angle of 173°) to show the effect of medium viscosity on particle diffusion. PMMA-grafted nanoparticles in solutions at 5 mg/mL were bath sonicated for about 2 min. The measurement time was set to 15 s, and data were averaged over 13 runs for three measurements at 25 °C. The refractive index of neat HMIM-TFSI is 1.4295 at 25 °C, and it is considered

https://dx.doi.org/10.1021/acs.jpcb.0c02813
J. Phys. Chem. B XXXX, XXX, XXX−XXX

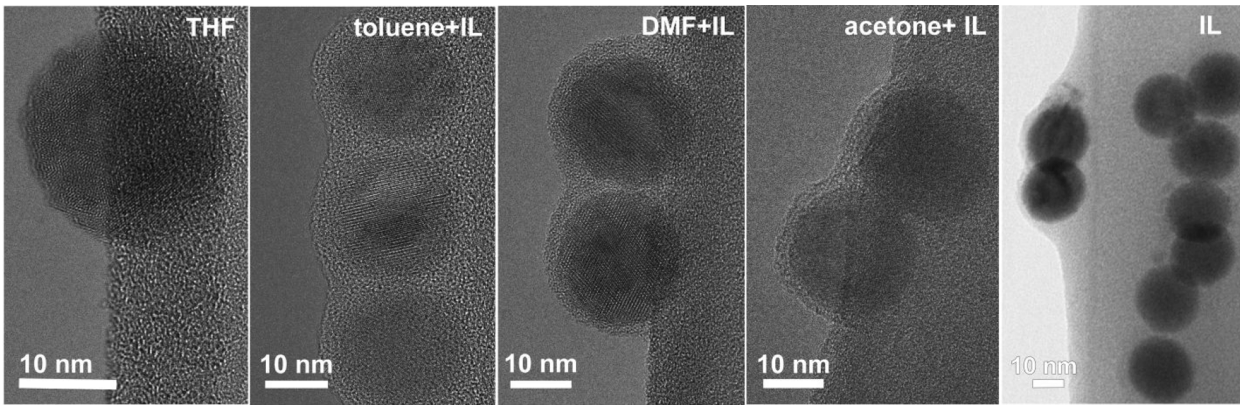

Figure 1. TEM images of 122.7 kDa PMMA-grafted Fe_3O_4 nanoparticles cast from pure THF, toluene−IL, DMF−IL, and acetone−IL mixtures as well as bare Fe_3O_4 in IL.

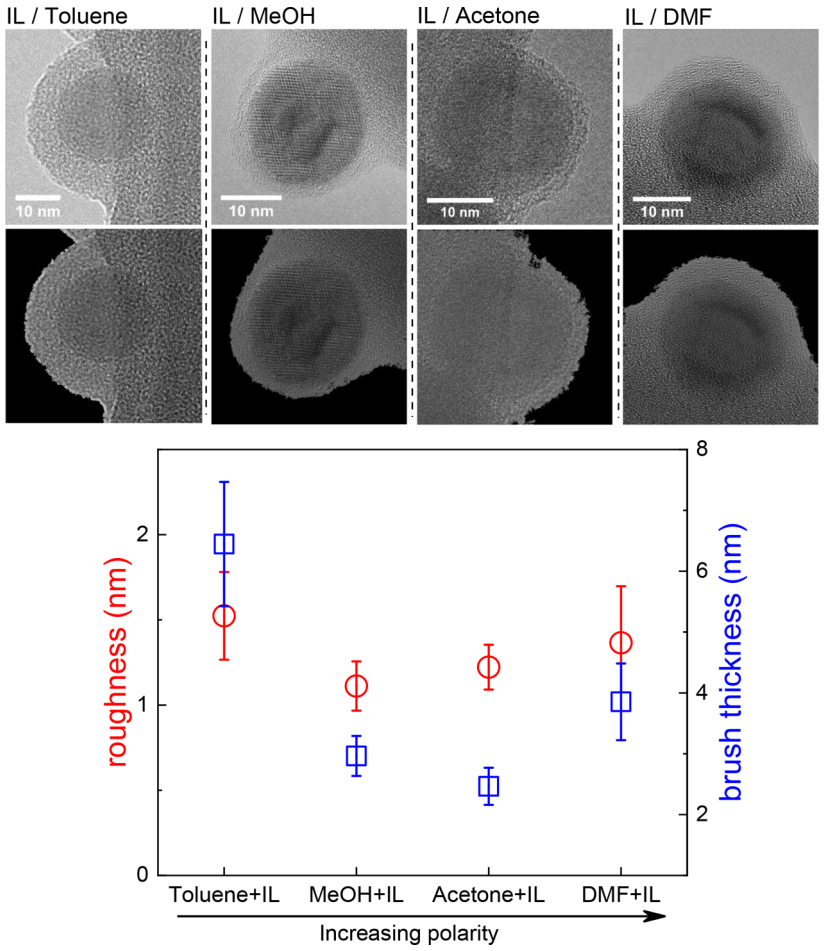

Figure 2. TEM images of PMMA-grafted particles (122.7 kDa, 0.7 chains/nm^2) cast from IL−solvent mixtures. A mask is applied to images to observe the rough boundaries of the IL-solvated brush layer. The roughness is shown in red and brush thickness in blue.

constant for solvent added IL mixtures. The viscosity (η) of neat HMIM-TFSI[41] is 70.09 mPa·s at 25 °C, and viscosities of HMIM-TFSI−solvent mixtures were measured by an ARES-G2 rheometer. Zero-shear viscosities used in dynamic light scattering (DLS) experiments are shown in Figure S1.

RESULTS AND DISCUSSION

Interparticle spacings and size distribution of nanoparticles are important parameters in colloidal and composite systems to understand the interactions of particles within medium, which are essential for stabilization of fillers in solution or bulk. IL is very stable under electron beam, and its nonvolatility enables imaging nanoparticles in ILs. In a recent work, a film cast from dilute suspensions of ILs on a lacey grid was imaged in electron microscopy, and particles were tracked as they diffused.[42] The thickness of IL on a lacey grid and strong adhesion of IL onto carbon-coated grids may affect the particle movements. In our study, thin films cast from dilute solutions of grafted particles in HMIM-TFSI were observed to be stationary, and particles did not diffuse as reported in Kim et al.'s work.[42]

https://dx.doi.org/10.1021/acs.jpcb.0c02813
J. Phys. Chem. B XXXX, XXX, XXX−XXX

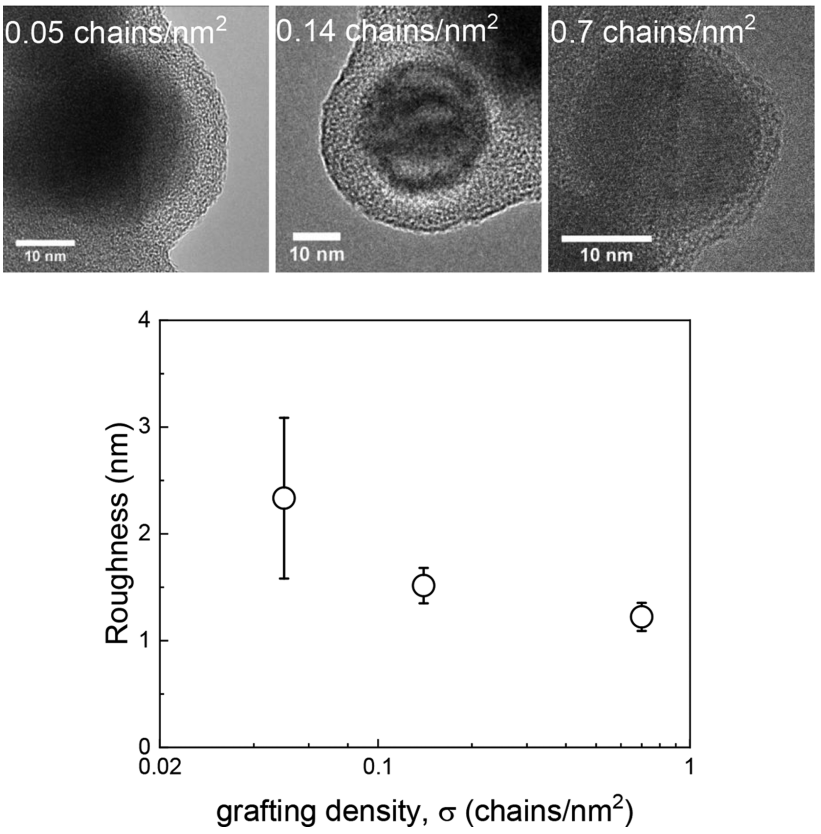

Figure 3. Calculated roughness of PMMA-grafted nanoparticles for different grafting densities (185.0 kDa with 0.05 chains/nm^2, 159.0 kDa with 0.14 chains/nm^2, and 122.7 kDa with 0.7 chains/nm^2). TEM images of drop-cast films from acetone−HMIM-TFSI mixtures.

The polymer becomes invisible when there is no IL in grafted particles (Figure 1). IL provides a good contrast to image the IL-solvated polymer chains around particles. The dense layer around nanoparticles depends on the extent of swelling of PMMA chains with IL. Figure 1 presents the TEM data of particles cast from IL−solvent mixtures. The thickness of IL solvated brush layers varied between 6.45 ± 1.02 and 2.46 ± 0.30 nm for films cast from IL−toluene and IL−acetone mixtures, respectively. We conjecture that the amount of IL within the interfacial layer increases as it swells the PMMA brushes, and this may influence the thickness and roughness of the brush layer, which is discussed in the following section. IL forms a thin layer on bare nanoparticles at a thickness roughly around 2.77 ± 0.59 nm, indicating the high wettability of IL to Fe_3O_4 particles (Figure 1). Additional TEM images of bare particles solvent cast from THF and HMIM-TFSI are included in Figure S2.

Surface roughness analysis of PMMA-grafted nanoparticles in HMIM-TFSI was performed by processing the TEM images in MATLAB.[43] The Image Segmented App applies a mask to a raw image to accurately isolate the brush boundary from background noise. The resulting binary image was then imported into MATLAB to obtain the brush boundary coordinates. Particle center to brush boundary distances were plotted versus interior angle to form a boundary profile for each image as shown in Figure S3. A perfect circle has a uniform flat boundary profile with no deviation in radius about its circumference. The brush thickness was calculated by subtracting the core radius from the radial distance of the boundary profile. The roughness and brush thickness of IL layers of the same grafted particles (122.7 kDa PMMA, $Đ$: 1.05 with 0.7 chains/nm^2 graft density) cast from IL−solvent mixtures are shown in Figure 2. The roughness and graft layer thickness analysis were done on 4−5 different particles. Figure S4 shows the representative data used in the image analysis. For a single particle, 500−4000 points were averaged for brush thickness analysis. A decrease in brush thickness from 6 to 2 nm was seen with increasing solvent polarity in IL−solvent mixtures (Figure 2). The brush thickness increased to 4 nm in the IL−DMF mixture which is attributed to the strong interactions between amide groups of DMF and carbonyl groups of PMMA,[44] resulting in better solvated PMMA by DMF. Overall, the brush thickness in IL−solvent solutions is influenced by both polymer−solvent and solvent−IL interactions. The roughness varies between 1.8 and 1.0 nm with the highest roughness of 1.8 nm in toluene−IL. In methanol−IL mixtures, PMMA brushes collapse because of poor solubility of PMMA in methanol. In the strongly solvated IL, the state in which polymer−IL interactions are stronger, it is proposed that counterions in IL may be ordered, resulting in higher electron density contrast in HMIM-TFSI, which contributes to the higher roughness values.

The roughness of particles with three different grafting densities (0.05, 0.14, and 0.7 chains/nm^2) is compared in Figure 3. The roughness is found to decrease with increasing graft density. We attribute the low roughness to the reduced swelling of PMMA brushes at 0.7 chains/nm^2 graft density. Figure S5 displays the TEM data used in the roughness analysis. Brush thickness can also be simply obtained by subtracting the core radius from the radius of grafted particle. This is repeated for several particles to get the averaged brush thicknesses as shown in Figure S6.

https://dx.doi.org/10.1021/acs.jpcb.0c02813
J. Phys. Chem. B XXXX, XXX, XXX−XXX

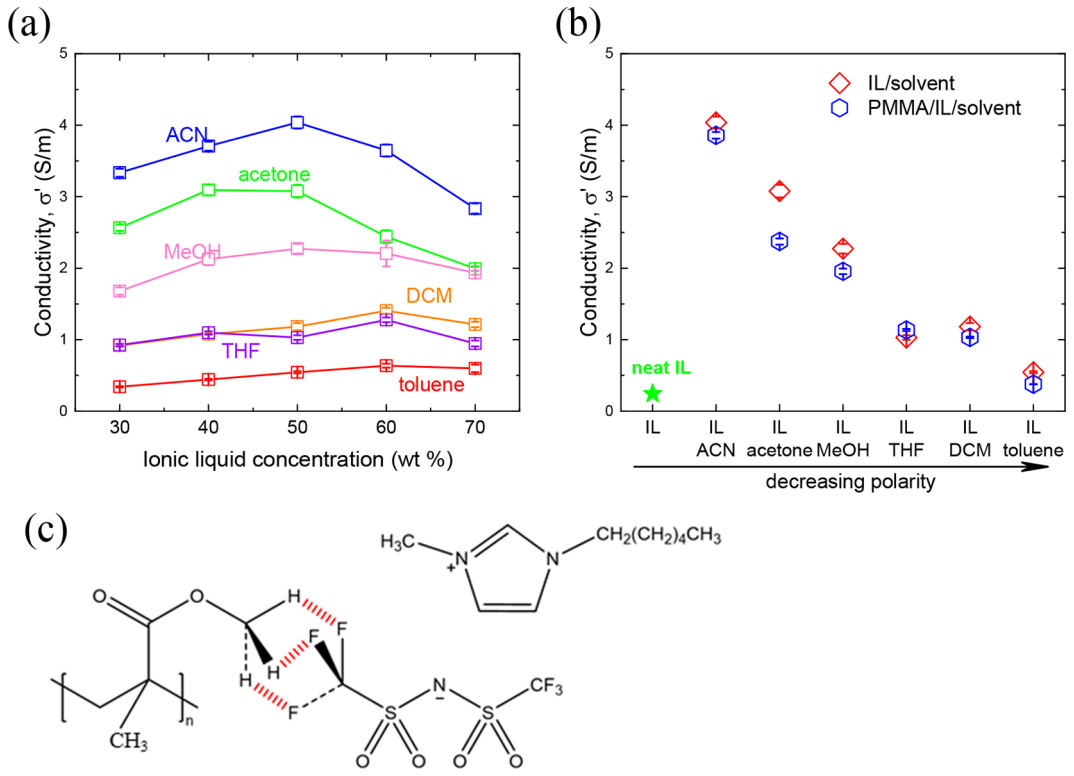

Figure 4. (a) Room temperature conductivity for selected solvents/IL (HMIM-TFSI) mixtures at varying IL concentrations. (b) Conductivity of IL−solvent mixtures with 0.5 wt % PMMA (118 kDa at 5 mg/mL). IL and solvent weight percentages are 49.75 and 49.75 wt %, respectively, in all mixtures. (c) Anion−dipole interactions between $TFSI^-$ and PMMA are depicted.

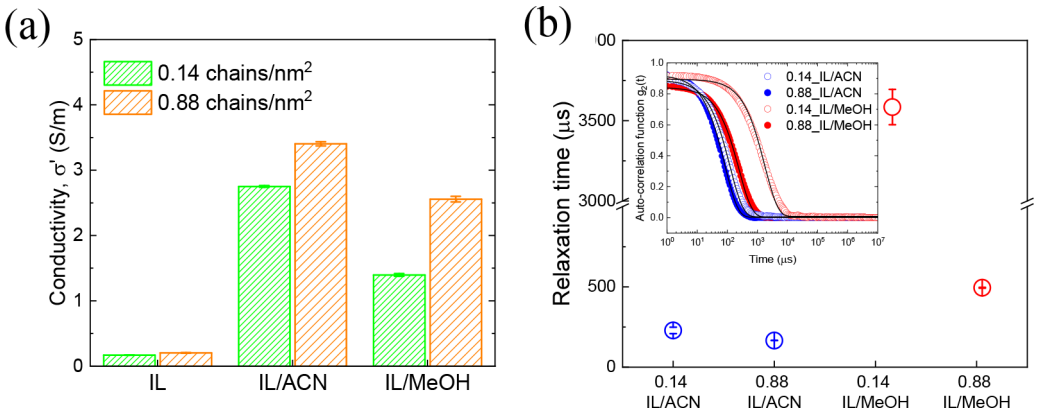

Figure 5. (a) Conductivity of IL−acetonitrile (ACN) and IL−methanol (MeOH) mixtures with PMMA grafted nanoparticles at 0.14 and 0.88 chains/nm^2. The grafted particle concentration is 0.4−0.5 wt %, and the mass ratio between IL and solvent is 1:1. (b) Relaxation times of PMMA grafted nanoparticles (42.2 kDa at 0.14 chains/nm^2 and 31.2 kDa at 0.88 chains/nm^2) in IL−acetonitrile and IL−methanol mixtures. The inset shows the normalized intensity−intensity time autocorrelation functions.

To further understand the solvation of IL with different solvents, conductivities of IL−solvent mixtures at various concentrations were measured. Adding solvents to the IL screens the electrostatic interactions between its ion pairs and leads to fast ion mobility, hence high conductivity. Acetonitrile, acetone, methanol, dichloromethane, THF, and toluene, listed in the order of decreasing polarity, were added to the IL. Figure 4a shows the IL concentration dependence of conductivities. Conductivity maxima were measured at intermediate concentrations (0.4−0.6 weight fraction of IL for all the six solvents chosen). This is consistent with the recent molecular dynamics simulations where the highest conductivity was shown for intermediate concentrations of the IL with the high polarity of solvents.[33] Acetonitrile, acetone, and methanol have the high dipole moments in decreasing order, and their conductivities correlate well with solvent polarity as seen in Figure 4a. In Figure 4b, conductivities of IL−solvent mixtures at 0.5/0.5 weight fraction are measured to be higher than that of the pure IL, which is expected due to the better solvation of IL with polar solvents. Adding 5 mg/mL of PMMA homopolymer (118 kDa), which is 0.5 wt % of the solution, into the IL−solvent mixtures did not change the conductivities as much compared to the pure IL−solvent mixtures (Figure 4b), even in methanol where PMMA has very low solubility. The weight percentages of PMMA/IL/solvent are 0.5/49.75/49.75. Additionally, we measured the con-

https://dx.doi.org/10.1021/acs.jpcb.0c02813
J. Phys. Chem. B XXXX, XXX, XXX−XXX

ductivity of IL−acetonitrile mixtures containing PMMA at varying concentrations. The conductivity dropped down from 4.0 to 2.7 S/m as PMMA concentration increased from 5 to 15 mg/mL (Figure S7). The conductivity reached a plateau above 15 mg/mL PMMA concentrations, in which the higher viscosity restricted the ion mobility.

After determining the optimal mixture composition, the ionic conductivities of IL/solvent mixtures with the PMMA-grafted nanoparticles were measured. The polymer-grafted particle concentration is ∼0.4−0.5 wt %, and the mass ratio between IL and solvent is kept to be 1:1 in all samples. The solubility of grafted chains in IL is critically important for the conformation of solvated chains. The ionic conductivities of IL with two different grafting density of particles (0.14 and 0.88 chains/nm^2) are found to be the same (Figure 5a). The conductivity was measured to be higher in HMIM-TFSI−acetonitrile for both grafting densities, whereas the higher grafting density particles presented the higher conductivity in both acetonitrile and methanol, suggesting that interactions between polymer−IL and solvent−IL contribute to the solvation. While PMMA is not soluble in methanol, the higher graft density sample still holds higher conductivity revealing the effect of solvent−IL interactions. The real part of the complex conductivity as a function of frequency for these two grafting densities samples in pure HMIM-TFSI, HMIM-TFSI−acetonitrile, and HMIM-TFSI−methanol mixtures is shown in Figure S8.

Solvent quality also affects the particle aggregation. We measured the diffusivity of particles in their IL−solvent mixtures using the Zetasizer NanoS instrument. Figure 5b presents the relaxation times of particles with 0.14 and 0.88 chains/nm^2 graft densities. Solutions contain 0.4−0.5 wt % of grafted nanoparticles and ∼50/50 wt % IL−solvent. Hydrodynamic size distributions are given in Figure S9. In a good solvent (acetonitrile, ACN), hydrodynamic sizes and relaxation times are quite similar for two grafting densities. In a poor solvent (methanol, MeOH), hydrodynamic size of low grafting density particles increases by a factor of 10, indicating clustering of nanoparticles. These results suggest that the nonaggregated particles in ACN can solvate IL through PMMA−IL mixing. Thus, IL−solvent solvation with the high grafting density particles yields high ionic conductivity. In conclusion, we demonstrate that in good solvent solvation is controlled by the two major interactions of polymer−IL and solvent−IL, whereas in poor solvent, solvent−IL interactions dictate high ion conductivity.

CONCLUSIONS

PMMA brushes solvated with HMIM-TFSI were imaged for the first time in transmission electron microscopy. The brush thickness and roughness parameters helped us to elaborate on the wetting characteristics of PMMA in IL. The swelling of brushes and the conductivities measured in the swollen and solvated states of grafted particles are reported. We found that brush roughness and thickness decrease with increasing polarity of solvent. The highest conductivity was measured with PMMA homopolymer in IL−acetonitrile. Conductivity results for the PMMA−IL−solvent mixtures suggest that preferential interactions between PMMA and HMIM-TFSI lead to conductivities higher than the pure HMIM-TFSI. Particles with dense brushes are found to be more conductive due to swelling of brushes with IL in acetonitrile, the solvent which is shown to solvate the IL effectively. The swelling of grafted chains with IL−solvent mixtures simultaneously leads to good stabilization of particles in solution. This study presents the stability of the PMMA-grafted particles in IL and explains the measured conductivities through the complex solvation between PMMA−IL and IL−solvents. These findings are unique since high ionic conductivities were obtained with the addition of grafted nanoparticles into IL through the solvation effect induced by dipolar interactions between polymer and IL.

ASSOCIATED CONTENT

Supporting Information

The Supporting Information is available free of charge at https://pubs.acs.org/doi/10.1021/acs.jpcb.0c02813.

Complex viscosity measured at varying shear rate; TEM images of bare nanoparticles; details of roughness analysis; TEM images of grafted nanoparticles cast from IL−solvent mixtures used in roughness analysis; comparison of brush thicknesses; ionic conductivity of IL−acetonitrile with PMMA homopolymer at varying concentrations; frequency dependence of complex conductivity; DLS data of grafted nanoparticles in IL−acetonitrile and IL−methanol (PDF)

AUTHOR INFORMATION

Corresponding Author

Pinar Akcora − *Department of Chemical Engineering & Materials Science, Stevens Institute of Technology, Hoboken, New Jersey 07030, United States;* orcid.org/0000-0001-7853-7201; Phone: (201) 216-5060; Email: pakcora@stevens.edu

Authors

Siqi Liu − *Department of Chemical Engineering & Materials Science, Stevens Institute of Technology, Hoboken, New Jersey 07030, United States*

Mia Walton − *Department of Chemical Engineering & Materials Science, Stevens Institute of Technology, Hoboken, New Jersey 07030, United States*

Nadezda V. Tarakina − *Department of Colloid Chemistry, Max Planck Institute of Colloids and Interfaces Research Campus Golm, Potsdam 14476, Germany;* orcid.org/0000-0002-2365-861X

Complete contact information is available at: https://pubs.acs.org/10.1021/acs.jpcb.0c02813

Notes

The authors declare no competing financial interest.

ACKNOWLEDGMENTS

This work was supported by the National Science Foundation DMR Polymers program under Award #1807802.

REFERENCES

(1) Brennecke, J. F.; Gurkan, B. E. Ionic Liquids for CO_2 Capture and Emission Reduction. *J. Phys. Chem. Lett.* **2010**, *1* (24), 3459−3464.

(2) Shi, W.; Luebke, D. R. Enhanced Gas Absorption in the Ionic Liquid 1-n-Hexyl-3-methylimidazolium Bis(trifluoromethylsulfonyl)-amide ([hmim][Tf2N]) Confined in Silica Slit Pores: A Molecular Simulation Study. *Langmuir* **2013**, *29* (18), 5563−5572.

(3) Ruckart, K. N.; O'Brien, R. A.; Woodard, S. M.; West, K. N.; Glover, T. G. Porous Solids Impregnated with Task-Specific Ionic

Liquids as Composite Sorbents. *J. Phys. Chem. C* **2015**, *119* (35), 20681−20697.
(4) Dyatkin, B.; Osti, N. C.; Gallegos, A.; Zhang, Y.; Mamontov, E.; Cummings, P. T.; Wu, J.; Gogotsi, Y. Electrolyte Cation Length Influences Electrosorption and Dynamics in Porous Carbon Supercapacitors. *Electrochim. Acta* **2018**, *283*, 882−893.
(5) Lin, R.; Huang, P.; Ségalini, J.; Largeot, C.; Taberna, P. L.; Chmiola, J.; Gogotsi, Y.; Simon, P. Solvent Effect on the Ion Adsorption from Ionic quid Electrolyte into Sub-nanometer Carbon Pores. *Electrochim. Acta* **2009**, *54* (27), 7025−7032.
(6) Largeot, C.; Portet, C.; Chmiola, J.; Taberna, P.-L.; Gogotsi, Y.; Simon, P. Relation Between the Ion Size and Pore Size for an Electric Double-Layer Capacitor. *J. Am. Chem. Soc.* **2008**, *130* (9), 2730−2731.
(7) Duan, X.; Ma, J.; Lian, J.; Zheng, W. The Art of Using Ionic Liquids in the Synthesis of Inorganic Nanomaterials. *CrystEngComm* **2014**, *16* (13), 2550−2559.
(8) Wang, L.; Chang, L.; Zhao, B.; Yuan, Z.; Shao, G.; Zheng, W. Systematic Investigation on Morphologies, Forming Mechanism, Photocatalytic and Photoluminescent Properties of ZnO Nanostructures Constructed in Ionic Liquids. *Inorg. Chem.* **2008**, *47* (5), 1443−1452.
(9) Migowski, P.; Machado, G.; Texeira, S. R.; Alves, M. C. M.; Morais, J.; Traverse, A.; Dupont, J. Synthesis and Characterization of Nickel Nanoparticles Dispersed in Imidazolium Ionic Liquids. *Phys. Chem. Chem. Phys.* **2007**, *9* (34), 4814−4821.
(10) Zhang, H.; Cui, H. Synthesis and Characterization of Functionalized Ionic Liquid-Stabilized Metal (Gold and Platinum) Nanoparticles and Metal Nanoparticle/Carbon Nanotube Hybrids. *Langmuir* **2009**, *25* (5), 2604−2612.
(11) Ueno, K.; Watanabe, M. From Colloidal Stability in Ionic Liquids to Advanced Soft Materials Using Unique Media. *Langmuir* **2011**, *27* (15), 9105−9115.
(12) Rodríguez-Arco, L.; López-López, M. T.; Durán, J. D. G.; Zubarev, A.; Chirikov, D. Stability and Magnetorheological Behaviour of Magnetic Fluids Based on Ionic Liquids. *J. Phys.: Condens. Matter* **2011**, *23* (45), 455101.
(13) Gao, J.; Ndong, R. S.; Shiflett, M. B.; Wagner, N. J. Creating Nanoparticle Stability in Ionic Liquid [C4mim][BF4] by Inducing Solvation Layering. *ACS Nano* **2015**, *9* (3), 3243−3253.
(14) Ueno, K.; Inaba, A.; Kondoh, M.; Watanabe, M. Colloidal Stability of Bare and Polymer-Grafted Silica Nanoparticles in Ionic Liquids. *Langmuir* **2008**, *24* (10), 5253−5259.
(15) Wittmar, A.; Ruiz-Abad, D.; Ulbricht, M. Dispersions of Silica Nanoparticles in Ionic Liquids Investigated with Advanced Rheology. *J. Nanopart. Res.* **2012**, *14* (2), 651.
(16) Ueno, K.; Imaizumi, S.; Hata, K.; Watanabe, M. Colloidal Interaction in Ionic Liquids: Effects of Ionic Structures and Surface Chemistry on Rheology of Silica Colloidal Dispersions. *Langmuir* **2009**, *25* (2), 825−831.
(17) Ueno, K. Soft Materials Based on Colloidal Self-assembly in Ionic Liquids. *Polym. J.* **2018**, *50* (10), 951−958.
(18) Ueno, K.; Fukai, T.; Nagatsuka, T.; Yasuda, T.; Watanabe, M. Solubility of Poly(methyl methacrylate) in Ionic Liquids in Relation to Solvent Parameters. *Langmuir* **2014**, *30* (11), 3228−3235.
(19) Ueno, K.; Sano, Y.; Inaba, A.; Kondoh, M.; Watanabe, M. Soft Glassy Colloidal Arrays in an Ionic Liquid: Colloidal Glass Transition, Ionic Transport, and Structural Color in Relation to Microstructure. *J. Phys. Chem. B* **2010**, *114* (41), 13095−13103.
(20) Ueno, K.; Inaba, A.; Sano, Y.; Kondoh, M.; Watanabe, M. A Soft Glassy Colloidal Array in Ionic Liquid, which Exhibits Homogeneous, Non-brilliant and Angle-Independent Structural Colours. *Chem. Commun.* **2009**, *24*, 3603−3605.
(21) Ueno, K.; Inaba, A.; Ueki, T.; Kondoh, M.; Watanabe, M. Thermosensitive, Soft Glassy and Structural Colored Colloidal Array in Ionic Liquid: Colloidal Glass to Gel Transition. *Langmuir* **2010**, *26* (23), 18031−18038.
(22) Unemoto, A.; Matsuo, T.; Ogawa, H.; Gambe, Y.; Honma, I. Development of All-Solid-State Lithium Battery Using Quasi-Solidified Tetraglyme-Lithium Bis(trifluoromethanesulfonyl)amide-Fumed Silica Nano-composites as Electrolytes. *J. Power Sources* **2013**, *244*, 354−362.
(23) Lu, Y.; Moganty, S. S.; Schaefer, J. L.; Archer, L. A. Ionic Liquid-Nanoparticle Hybrid Electrolytes. *J. Mater. Chem.* **2012**, *22* (9), 4066−4072.
(24) Huang, Y.; Takata, A.; Tsujii, Y.; Ohno, K. Semisoft Colloidal Crystals in Ionic Liquids. *Langmuir* **2017**, *33* (28), 7130−7136.
(25) Scott, M. P.; Rahman, M.; Brazel, C. S. Application of Ionic Liquids as Low-Volatility Plasticizers for PMMA. *Eur. Polym. J.* **2003**, *39* (10), 1947−1953.
(26) Scott, M. P.; Brazel, C. S.; Benton, M. G.; Mays, J. W.; Holbrey, J. D.; Rogers, R. D. Application of Ionic Liquids as Plasticizers for Poly(methyl methacrylate). *Chem. Commun.* **2002**, *13*, 1370−1371.
(27) Susan, M. A. B. H.; Kaneko, T.; Noda, A.; Watanabe, M. Ion Gels Prepared by in Situ Radical Polymerization of Vinyl Monomers in an Ionic Liquid and Their Characterization as Polymer Electrolytes. *J. Am. Chem. Soc.* **2005**, *127* (13), 4976−4983.
(28) Kofu, M.; Someya, T.; Tatsumi, S.; Ueno, K.; Ueki, T.; Watanabe, M.; Matsunaga, T.; Shibayama, M.; Sakai, V. G.; Tyagi, M.; Yamamuro, O. Microscopic Insights into Ion Gel Dynamics Using Neutron Spectroscopy. *Soft Matter* **2012**, *8* (30), 7888−7897.
(29) Osti, N. C.; Van Aken, K. L.; Thompson, M. W.; Tiet, F.; Jiang, D.-e.; Cummings, P. T.; Gogotsi, Y.; Mamontov, E. Solvent Polarity Governs Ion Interactions and Transport in a Solvated Room-Temperature Ionic Liquid. *J. Phys. Chem. Lett.* **2017**, *8* (1), 167−171.
(30) Tokuda, H.; Baek, S.-J.; Watanabe, M. Room-Temperature Ionic Liquid-Organic Solvent Mixtures: Conductivity and Ionic Association. *Electrochemistry* **2005**, *73* (8), 620−622.
(31) Li, W.; Zhang, Z.; Han, B.; Hu, S.; Xie, Y.; Yang, G. Effect of Water and Organic Solvents on the Ionic Dissociation of Ionic Liquids. *J. Phys. Chem. B* **2007**, *111* (23), 6452−6456.
(32) Fox, E. T.; Paillard, E.; Borodin, O.; Henderson, W. A. Physicochemical Properties of Binary Ionic Liquid−Aprotic Solvent Electrolyte Mixtures. *J. Phys. Chem. C* **2013**, *117* (1), 78−84.
(33) Thompson, M. W.; Matsumoto, R.; Sacci, R. L.; Sanders, N. C.; Cummings, P. T. Scalable Screening of Soft Matter: A Case Study of Mixtures of Ionic Liquids and Organic Solvents. *J. Phys. Chem. B* **2019**, *123* (6), 1340−1347.
(34) Liu, S.; Liedel, C.; Tarakina, N. V.; Osti, N. C.; Akcora, P. Dynamics of Ionic Liquids in the Presence of Polymer-Grafted Nanoparticles. *Nanoscale* **2019**, *11* (42), 19832−19841.
(35) Park, J.; An, K.; Hwang, Y.; Park, J.-G.; Noh, H.-J.; Kim, J.-Y.; Park, J.-H.; Hwang, N.-M.; Hyeon, T. Ultra-Large-Scale Syntheses of Monodisperse Nanocrystals. *Nat. Mater.* **2004**, *3*, 891−895.
(36) Sun, S.; Zeng, H.; Robinson, D. B.; Raoux, S.; Rice, P. M.; Wang, S. X.; Li, G. Monodisperse MFe_2O_4 (M = Fe, Co, Mn) Nanoparticles. *J. Am. Chem. Soc.* **2004**, *126*, 273−279.
(37) Li, C.; Han, J.; Ryu, C. Y.; Benicewicz, B. C. A Versatile Method To Prepare RAFT Agent Anchored Substrates and the Preparation of PMMA Grafted Nanoparticles. *Macromolecules* **2006**, *39*, 3175−3183.
(38) Jiao, Y.; Akcora, P. Assembly of Polymer-Grafted Magnetic Nanoparticles in Polymer Melts. *Macromolecules* **2012**, *45*, 3463−3470.
(39) Di Noto, V.; Vittadello, M.; Lavina, S.; Fauri, M.; Biscazzo, S. Mechanism of Ionic Conductivity in Poly(ethyleneglycol 400)/(LiCl)x Electrolytic Complexes: Studies Based on Electrical Spectroscopy. *J. Phys. Chem. B* **2001**, *105* (20), 4584−4595.
(40) Singh, M.; Odusanya, O.; Wilmes, G. M.; Eitouni, H. B.; Gomez, E. D.; Patel, A. J.; Chen, V. L.; Park, M. J.; Fragouli, P.; Iatrou, H.; Hadjichristidis, N.; Cookson, D.; Balsara, N. P. Effect of Molecular Weight on the Mechanical and Electrical Properties of Block Copolymer Electrolytes. *Macromolecules* **2007**, *40* (13), 4578−4585.
(41) Tariq, M.; Forte, P. A. S.; Gomes, M. F. C.; Lopes, J. N. C.; Rebelo, L. P. N. Densities and Refractive Indices of Imidazolium- and Phosphonium-Based Ionic Liquids: Effect of Temperature, Alkyl

https://dx.doi.org/10.1021/acs.jpcb.0c02813
J. Phys. Chem. B XXXX, XXX, XXX−XXX

Chain Length, and Anion. *J. Chem. Thermodyn.* **2009**, *41* (6), 790−798.
(42) Kim, P. Y.; Ribbe, A. E.; Russell, T. P.; Hoagland, D. A. Visualizing the Dynamics of Nanoparticles in Liquids by Scanning Electron Microscopy. *ACS Nano* **2016**, *10* (6), 6257−6264.
(43) Wang, Y. C.; Slater, T. J. A.; Rodrigues, T. S.; Camargo, P. H. C.; Haigh, S. J. Automated Quantification of Morphology and Chemistry from STEM Data of Individual Nanoparticles. *J. Phys.: Conf. Ser.* **2017**, *902*, No. 012018.
(44) Patra, N.; Barone, A. C.; Salerno, M. Solvent Effects on the Thermal and Mechanical Properties of Poly(methyl methacrylate) Casted from Concentrated Solutions. *Adv. Polym. Technol.* **2011**, *30* (1), 12−20.

https://dx.doi.org/10.1021/acs.jpcb.0c02813
J. Phys. Chem. B XXXX, XXX, XXX−XXX